Environmental Earth Sciences (2018) 77:747
https://doi.org/10.1007/s12665-018-7938-9

ORIGINAL ARTICLE

Hydrogeochemical and environmental isotopes study of the northeastern Algerian thermal waters

Yassine Gueroui[1,2] · Ammar Maoui[2] · Hassen Touati[3] · Mohamed Guettaf[4] · Aissam Bousbia[4]

Received: 20 June 2018 / Accepted: 1 November 2018 / Published online: 15 November 2018

Abstract

Thermal waters from northeastern Algeria have been investigated for their hydrochemical and isotopic characteristics to identify the geothermal processes that have produced these waters. Fifteen samples were collected from cold and hot springs. The data obtained from sampling period indicate a high level of mineralization (a TDS of up to 6657 mg/L) of thermal waters with three dominant water types (Ca–SO_4, Ca–HCO_3, Na–Cl). The chemical geothermometers applied to thermal waters show that the study area is influenced in part through dilution by the infiltration of surface waters. The isotopic contents of hot springs vary from −8.26 to −6.83‰ for $\delta^{18}O$ and from −55.23‰ to −42.01‰ for $\delta 2H$. These results reveal a meteoric origin of thermal waters infiltrated at major faults and heated by deep flow before being discharged to the surface by fractures.

Keywords Thermal waters · Northeastern Algeria · Hydrogeochemistry · Mineral saturation · Environmental isotopes · Geothermometry

Introduction

Since Roman times, thermal waters have been used for different purposes due to their therapeutic properties. Most of these waters are located in volcanic areas all over the world reflecting the influence of long-lived hydrothermal systems (Wohletz and Heiken 1992; Asta et al. 2012; Amarouche-Yala et al. 2014).

A number of previous studies have been undertaken to investigate the hydrogeological, physicochemical and bacteriological characteristics of thermal waters in Algeria (Verdeil 1982; Dib 1985; Issaadi 1992; Bouchareb-Haouchine 1993; Kedaid and Mesbah 1996; Bouchareb-Haouchine et al. 2012; Amarouche-Yala et al. 2014; Belhai et al. 2016, 2017). There are more than 240 thermal springs in Algeria, 70 of which are concentrated in the northeastern part of the country that have discharge temperatures that vary from 31 to 98 °C. These thermal springs are often used in spas and are, therefore, are of great social and economic importance (Issaadi 1992; Bouchareb-Haouchine 1993; Kedaid and Mesbah 1996; Kedaid 2007; Kecha et al. 2007; Bouanane-Darenfed et al. 2011; Belhai et al. 2017).

The study area is one of the important geothermal areas in Algeria. It is located northeast of Algiers and belongs to the Maghrebide-Alpine chain of North Africa. It is a part of a peri-Mediterranean Alpine region of Tertiary age. Many thermal springs in this area are used in public baths. They have heterogeneous temperatures reaching 98 °C in Hammam Debagh considered as the highest temperature in the country and the second over the world.

Many methods have been used to understand the geothermal systems of the study area including the application of hydrogeochemical and isotopic techniques. The chemical and isotopic composition and the geothermometer methods provide us with information about the origin of fluids, their flow path, recharge areas and the reservoir temperature. The present study is a contribution to understanding hydrochemical processes in both hot and cold water in thermal areas. The principal aims of this research are as follows: (1) to have a better understanding of the water chemistry and the

✉ Yassine Gueroui
gueroui.yassine@univ-guelma.dz

[1] Département des Sciences de la Nature et de la Vie, Université 8 Mai 1945 Guelma, BP 401, 24000 Guelma, Algeria

[2] Laboratoire Génie Civil et Hydraulique (LGCH), Université 8 Mai 1945 Guelma, BP 401, 24000 Guelma, Algeria

[3] Laboratoire Eco-biologie des Milieux Marins et Littoraux, Université Badji Mokhtar, Annaba, Algeria

[4] Laboratoire Biologie, Eau et Environnement, Université 8 Mai 1945 Guelma, BP 401, 24000 Guelma, Algeria

interactions with the host rock, (2) to infer the temperatures of the reservoir using geothermometers, and (3) to define the origin of thermal waters using environmental isotopes.

Study area

General framework

The study area is located in the northeastern part of Algeria, nearly 600 km to the east of Algiers and 60 km to the south of the Mediterranean Sea. The study area constitutes a meeting point between six wilaya and covers an area of 4101 km (Fig. 1). This region is characterized by the presence of a large number of thermal water sources of variable importance, including the Debagh and Hammam Ouled Ali hot springs which are known for their healing properties. The temperature of these thermal waters varies between 37.6 and 91.9 °C. The region has a Mediterranean climate, characterized by a mild rainy winter and a hot summer. The temperature in the region varies from 4 °C in winter to 35.4 °C in summer with an annual average of 17.3 °C. The annual precipitation ranges between 400 and 500 mm in the southern part of the area and can reach 1000 mm per year in the north. A total of 57% of this rainfall is recorded during the period from October to May. This resulted in subhumid climate in the center and northern parts of the study area and semi-arid climate in the south (ANDI 2013).

Geological setting

The geology of the study area has been described by several authors (Deleau 1952; Vila 1966; Vila et al. 1968, 1972; Vila and Magne 1969; Vila 1970, 1980; Vila and Ailloud 1978; Lahondère et al. 1979; Lahondère 1987; Chouabbi 1987).

The study area belongs to the geological set of the external Tell. They are, from top to bottom, the Quaternary, the Mio-Pliocene, the Numidian domain, the flysch formations, the Tellian domain, the Ultra-Tellian domain, the scales of the Sellaoua and finally the Constantine Neritic formations (Fig. 2).

The Quaternary formations are located along the Seybouse Valley and represented by terraces: the lower terrace (Solatnian), the middle terrace (Tensiftian) and the higher terrace (Saletian). These terraces are generally nested but can let appear the marly gypsifer substratum between them (Vila 1980).

The Mio-Pliocene formations are gray clays with intercalations of marl-limestone and gypsum in thin layers. They surmount clays and red conglomerates.

The Numidian domain constitutes the tops of the reliefs, marked by a clay–sandstone facies. The base of these series

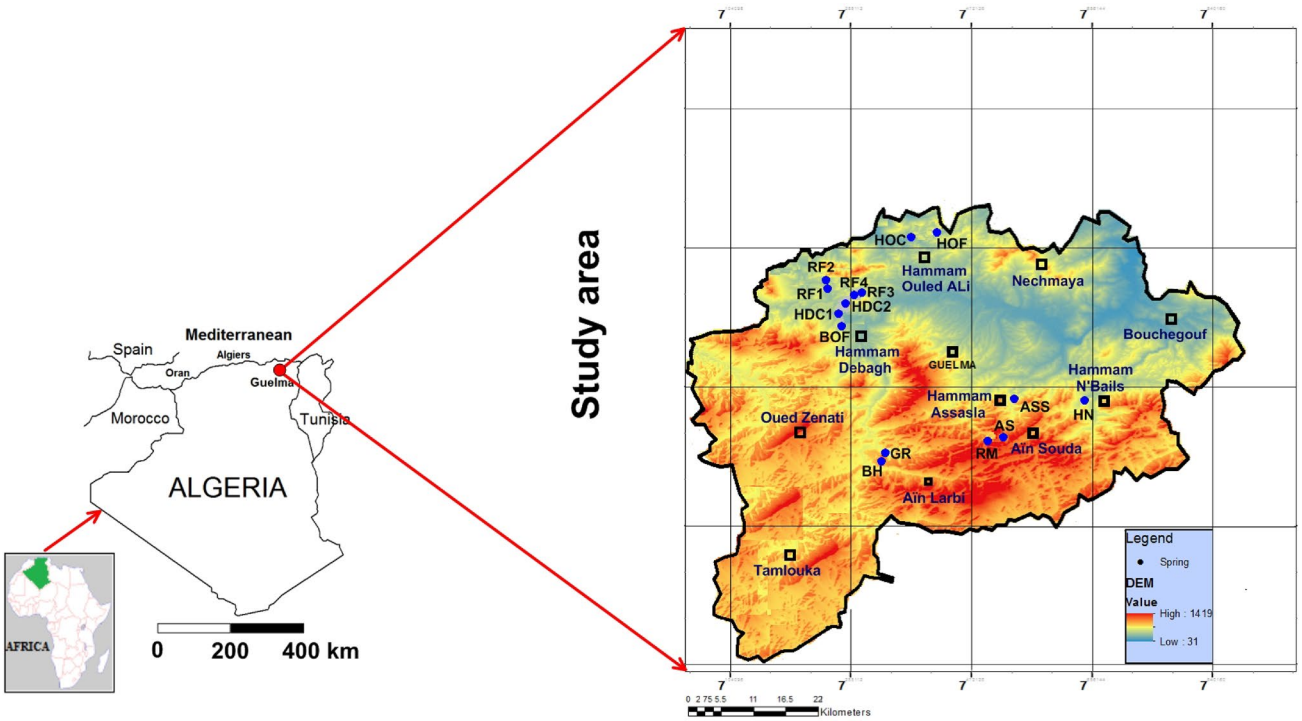

Fig. 1 Location of the study area

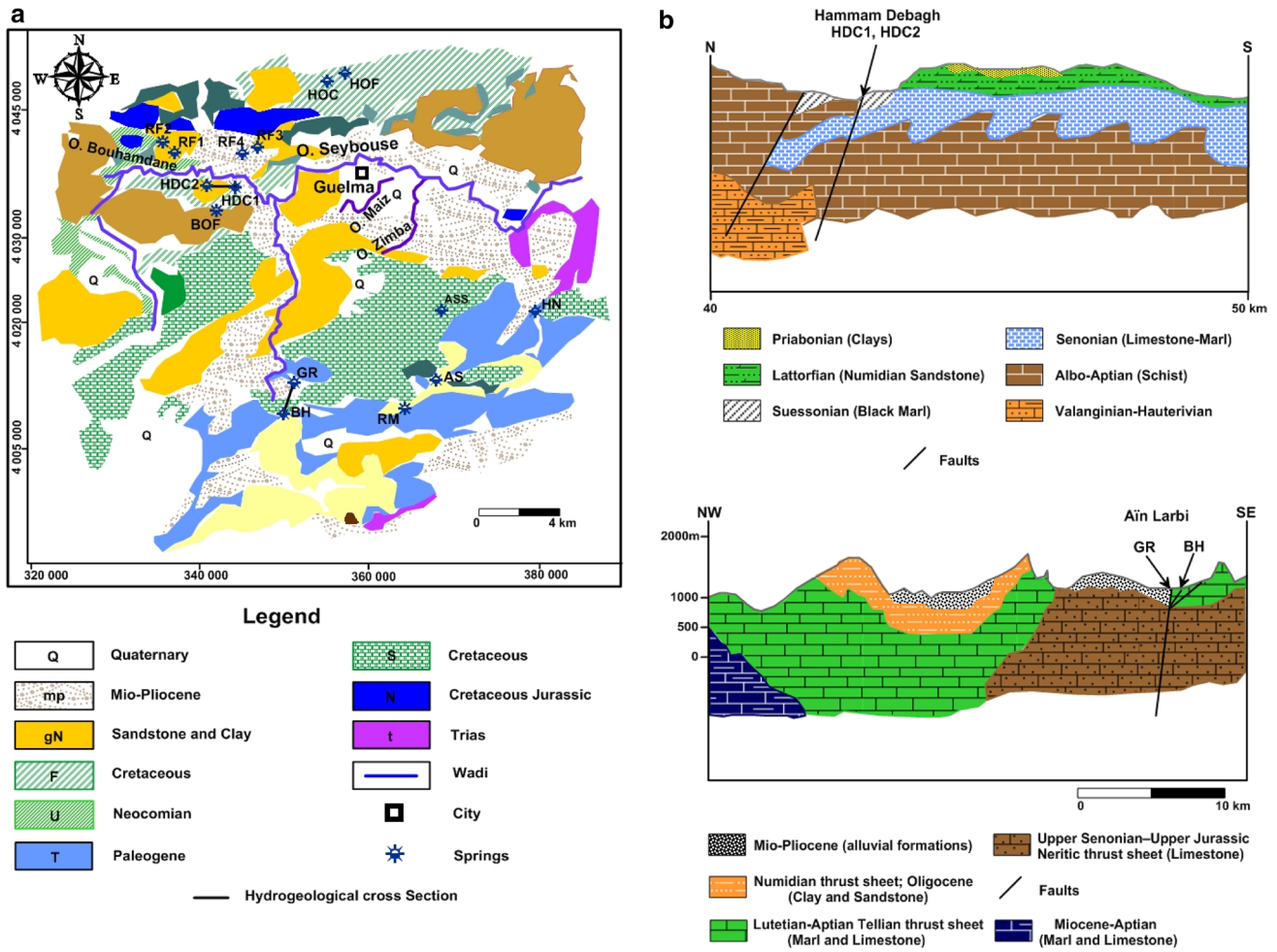

Fig. 2 **a** Geological map of the northeastern Algeria, **b** Hydrogeological cross-section through Hammam Debagh and Aïn Larbi

is represented by clays (Tubotomaculum) of middle-to-upper Oligocene age and surmounted by a thick sandstone series of Aquitanian age (Lahondère et al. 1979; Vila 1980).

The flysch formations appear under the clay–sandstone facies of the Numidian domain. There are the Senonian which is a conglomerate and argillaceous series representing the meridional facies of flysh and the Cenomanian–Turonian represented by clear brecciated levels classified in white silicified bands. These formations are dated by *Rotalipora* sp., *Thalmanninella* sp. and *Globotrucana helvética*. The Lower Cretaceous is a series with gray or brownish clay–schist intercalations. At the base, it shows some limestone deposits (*Nannoconus*) (Vila 1966).

The Tellian domain is the external Tell domain made up of the Paleogene formations. They are a thick series with dominant marly of the furrow Tellian. The Ultra-Tellian domain refers to the series superimposed abnormally on the Constantine neritic Cretaceous in the region of Guelma. These series are defined by the dominance of clear facies throughout the Cretaceous (Durand Delga 1969).

The scales of the Sellaoua are the external tell domain made up of the Paleogene formations. There are the Tellian units at Globigerins which include a Paleocene made up of marls, a Ypresian with limestones and (Globigerins) and a lower to medium Lutetian with black marls and yellow carbonates; the Tellian unit at Nummulites include a Paleogene with black marls and a massive Eocene limestone with Nummulites surmounted by a marly series of Lutetian age.

The Neritic Constantine Neritic formations in the region of Guelma represent the eastern endpoint of the Neritic domain. These formations are isolated and of variable sizes (Vila et al. 1972).

Structural framework

The current structure of the study area is the result of a series of tectonic movements. The different phases are the finite-Eocene phase called “atlasic” which marks the end of a large sedimentation cycle in the Maghreb basin that began with deposits from the Upper Triassic to the Lutetian. It is

responsible for the creation of the flyschs and the Tellian. The lower Miocene phase is responsible for the birth of the current building. In the post-nappe tectonic phase from Tortonien to the current, the area is known for the set of several deformations that have succeeded or combined. These accidents have drawn a spectacular network of faults of atlasic direction (NE–SW). It can be noted that the thermo-mineral springs are located along the directional faults (NE–SW and North–South) (Vila 1980).

Sampling and analytical methods

Water samples were collected during January 2017 from fifteen hot and cold springs to determine their hydrogeochemical and isotopic composition. The seven thermal springs and the eight cold water samples were collected from different locations in the province of Guelma including Hammam Debagh, Hammam Ouled Ali, Hammam N'Bails, Hammam A > ssasla, Aïn Souda and Aïn Larbi. Measurements of temperature, electrical conductivity, total dissolved solids (TDS), pH and dissolved oxygen were made in the field using a Multiparameter WTW set (Multiline P3 PH/LF SET), and an oxymeter (WTW) with an oxygen probe (CellOX 325). Chemical analyses were conducted at the "Laboratoire de Radio-Analyses et Environment" of the "Ecole Nationale d'Ingénieurs de Sfax", Tunisia and Civil Engineering and Hydraulic Laboratory, University, 8 May 1945, Guelma, Algeria. Samples for major ion and isotopic analyses were collected in polyethylene and glass bottles, respectively, and stored at 4 °C until laboratory analysis. Ca^{2+}, Mg^{2+}, Na^{+}, K^{+}, Cl^{-}, and $SO_4{}^{-2}$ were measured using ion liquid chromatography (ILC) equipped with columns IC-Pak TM CM/D for cations using EDTA and nitric acid an eluant, and on a Metrohm chromatograph equipped with columns CI SUPER-SEP for anions using phthalic acid and acetonitrile an eluant. Alkalinity measurements were determined by titration with the methyl orange endpoint. $NO_3{}^{-}$ and SiO_2 were determined by colorimetric method. Stable isotopes ($\delta^{18}O$, $\delta^{2}H$) were analyzed using the Laser Absorption Spectrometer LGR DLT 100 (Penna et al. 2010). The results were reported to the V-SMOW standard (Vienna Standard Mean Ocean Water). The ionic balance error of all samples was determined to be within the acceptable limit of ±5%. The hydrochemical calculations were performed using DIAGRAMMES program. Geothermometers were used to determine the temperatures of the geothermal systems.

Results and discussion

Water chemistry

The results of physical and chemical analyses of thermal and cold waters are reported in Table 1.

The temperature of the thermal waters ranged from 27.6 °C in Hammam Assasla spring to 91.9 °C found in Hammam Debagh which is considered as the hottest spring in Algeria, while the cold waters showed temperatures that ranged from 14 to 17.7 °C. Both the thermal and cold waters showed near-neutral pH values ranging from 7.13 to 7.84 and from 7.45 to 8.06, respectively. The electrical conductivity

Table 1 Chemical composition (mg/L) of collected hot and cold springs of northeastern Algeria

Samples ID	T (°C)	pH	EC	TDS	O_2	Ca^{2+}	Mg^{2+}	Na^{+}	K^{+}	$HCO_3{}^{-}$	Cl^{-}	$SO_4{}^{2-}$	SIO_2	$NO_3{}^{-}$	Ionic balance (%)
RF1	14.2	7.67	801	517.52	3.51	104.46	6.52	25.25	5.02	244	61.01	21.63	4.74	49.65	0
RF2	17.7	7.73	782	575.07	7.15	113.54	7.45	27.63	24.46	237.9	87.78	20.41	4.94	55.92	3
RF3	14.3	7.79	549	403.25	7.6	67.25	11.43	30.90	1.66	225.7	36.24	24.83	4.88	5.26	3
RF4	14.9	8.06	1225	849.13	7.56	44.51	78.28	84.64	5.33	469.7	91.31	62.00	4.80	13.36	3
BOF	17.1	7.45	2510	1954.10	1.83	425.90	17.46	82.98	91.08	122	207.58	963.92	6.12	43.18	0
AS	14.7	7.68	495	355.43	0.03	67.13	13.24	10.12	1.96	219.6	16.39	15.09	3.39	11.91	4
RM	14	7.62	425	316.95	3.26	59.20	12.36	9.38	1.16	183	15.80	23.77	3.23	12.30	3
HOF	14.3	7.78	649	506.46	6.5	111.46	8.02	23.23	1.15	280.6	44.63	32.79	3.76	4.60	5
ASS	27.6	7.82	709	527.10	0.19	101.09	18.74	25.10	3.29	225.7	42.90	110.29	5.86	0.00	4
HN	37.6	7.13	9720	6657.40	0.22	594.20	82.60	1582.50	87.10	671	3192.40	447.60	9.23	0.00	– 1
GR	45.2	7.79	2370	1718.90	5.7	345.20	56.96	114.52	13.80	122	231.60	834.82	22.70	0.00	2
HOC	53.6	7.84	1342	960.19	1.87	198.86	33.48	33.70	8.70	268.4	43.14	373.91	21.40	0.00	4
BH	61.9	7.41	2470	1873.98	0.18	394.68	59.86	117.82	16.10	183	240.52	862.00	22.95	0.00	4
HDC1	91.9	7.76	2180	1488.82	1.65	190.44	30.90	205.74	24.72	251.1	388.72	387.32	33.35	9.88	– 4
HDC2	80.6	7.41	2280	1566.78	2.11	205.96	29.38	211.22	23.06	347.7	374.84	374.62	31.00	0.00	– 3

EC electrical conductivity (µS/cm), *TDS* total dissolved solids

values of water samples varied between 709 and 9720 µS/cm for thermal springs and between 425 and 2510 µS/cm for cold springs. Cold waters were generally oxygenated while the thermal waters presented low dissolved oxygen concentration except for Hammam Guerfa (GR) which showed a moderate value of 5.7 mg/L. According to the Piper diagram (Fig. 3), there are three different types of waters in the study area. The majority of the thermal springs (GR, HOC, BH, HDC1, HDC2) are sulfate waters with higher Ca–SO_4 contents and an average TDS value of 1521.73 mg/L, while the most of cold springs (RF1, RF2, RF3, RF4 AS, RM, HOF) are bicarbonate waters rich in Ca–HCO_3 contents with an average TDS value of 509.83 mg/L. However, there were two hot springs with differing compositions, those are (HN) with a chloride dominant chemical composition with higher Na–Cl contents and (ASS) with bicarbonate water type. Additionally, one cold spring (BOF) has a sulfate dominant composition. The chemical composition of sulfate and chloride waters reveals the influence of the evaporitic host rocks rich in gypsum and halite, while the bicarbonate composition of waters may be due to interactions of meteoric water with limestone and dolomite (Belhai et al. 2017). The high TDS values of thermal waters compared to the cold waters may reflect a longer circulation and residence times (Bozdağ 2016). In the thermal waters, sodium appeared as the dominant cation (1582.50 mg/L) followed by calcium (594 mg/L) and chloride is the dominant anion (3192 mg/L) followed by sulfate (862 mg/L), while in the cold waters the dominant cation is calcium (426 mg/L) and the dominant anion is sulfate (964 mg/L).

Calcium and magnesium concentrations in water samples ranged from 45 to 594 mg/L and from 7 to 83 mg/L, respectively. The main origin of these ions is the dissolution of carbonate minerals. The concentrations obtained for Na and K varied between 9–1582 and 1–87 mg/L, respectively. Chloride concentrations ranged from 16 to 3192 mg/L. These concentrations may be due to the alteration of sandstone and clay of the Numidian, and also to the presence of the ion exchange process with calcium (Langmuir 1997; Fourré et al. 2011; Belhai et al. 2017). The concentration values of bicarbonate varied between 122 and 671 mg/L. The values of sulfate ranged from 15 to 862 mg/L. The main sources of sulfate are likely to be from the dissolution of gypsum and the oxidation of sulfide minerals (Amarouche-Yala et al. 2014). A high concentration value of NO_3 was found in cold waters ranging from 5 to 56 mg/L, while in thermal waters

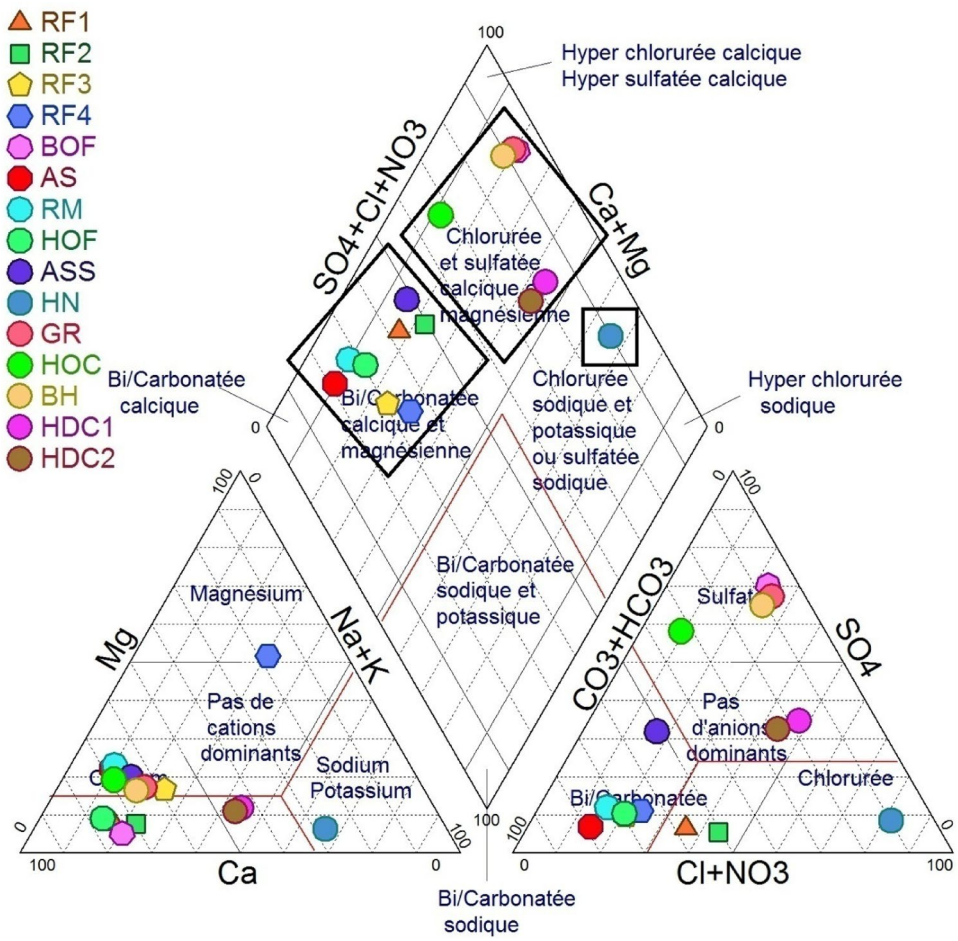

Fig. 3 Piper diagram of water chemistry in the study area

the values are below detection except for one spring (HDC1) which showed a value of 10 mg/L. These concentrations values may be due to the influence of anthropogenic and agricultural activities as well as the phenomenon of infiltration.

Chloride is one of the most elements used as tracers for hydrological cycle studies because of its conservative nature and their weak interaction with the host rock (Michard 1990; Boudoukha and Athamena 2012). The chloride concentrations versus Ca, Mg, Na, K, and HCO_3 are shown in the scatter diagram (Fig. 4). The thermal waters of the study area show a strong positive correlation with the straight line of halite dissolution between Na–Cl ($R^2 = 0.9$), K–Cl ($R^2 = 0.7$) and HCO_3–Cl ($R^2 = 0.5$). At the same time, a positive correlation is noted between Ca–Cl ($R^2 = 0{,}66$) and Mg–Cl ($R^2 = 0{,}56$). As a result, this positive correlation may be explained by the mixing and dilution process of thermal waters by the infiltrating shallow cold waters which interact with the Triassic evaporates (Alçiçek et al. 2016; Belhai 2017).

Geothermometry applications

Thermal reservoir temperatures are an important tool that allows the assessment of the formation mechanism and potential use of geothermal resources. Several geothermometers based on the temperature-dependent chemical equilibria have been developed to evaluate the geothermal reservoir temperatures (Trabelsi et al. 2015; Bozdağ 2016; Belhai et al. 2016, 2017). The reservoir temperatures of Guelma thermal waters were estimated by the following geothermometers: silica: quartz (Fournier 1977), chalcedony (Fournier 1977), cristobalite (α) (Fournier 1977) and cation: Na–K (Michard 1979), Na–K (Fournier 1977), Na–K (Truesdell 1976) and Na–K–Ca (Benjamin et al. 1983). The silica concentrations are expressed in mg/l and Na, K and Ca concentrations in mol/l. As shown in Table 2 and Fig. 5, the lowest estimated reservoir temperatures are given by the silica geothermometers (Fig. 5b) in contrast to the highest temperatures calculated by cationic geothermometers (Fig. 5a). Water temperatures estimated at the origin using the silica geothermometers vary between 17 and 84 °C. The temperatures obtained by quartz geothermometers appear higher and more plausible than chalcedony and cristobalite (α) geothermometers. However, the low estimated temperatures of silica geothermometers could be due to the silica precipitation or the mixing process (Boudoukha and Athamena 2012; Belhai et al. 2017).

The cationic geothermometers provides high temperature values ranging from 91 to 325 °C. The values higher than temperatures at emergence show a dissipation during the upwelling from the reservoir to the surface. This dissipation could be due to several assumptions: a mixture with cold water, the thermal diffusion linked to the long path travelled by these waters to the surface, the loss of Ca by precipitation of calcite or to the high Mg contents indicating surface reactions with the rocks (Boudoukha and Athamena 2012; Belhai et al. 2017).

Na–K–Mg diagram

The ternary diagram of Na/1000-K/100-$Mg^{1/2}$ (Fig. 6) proposed by Giggenbach (1988) was used to estimate the reservoir temperatures and to differentiate between mature and immature waters along their flow paths (Ersoy and Sönmez 2014). The diagram applied for this study shows that thermal samples are concentrated at the magnesium pole indicating the waters are immature. This may suggest that the thermal waters of the study area are influenced by high dilution and mixing with shallow cold waters (Boucharef-Haouchine et al. 2012).

Mineral saturation

The geochemical program PHREEQ-C (Parkhurst and Apello 1999) was used to calculate mineral saturation indices of thermal waters from the study area at the outlet temperatures and pH values. The results are presented in Table 3. A saturation index of zero indicates an equilibrium state for each mineral reacting with aqueous solution. Positive or negative SI values correspond to oversaturation or undersaturation, respectively (Gökgöz and Akdağoğlu 2016). The thermal waters of the study area are oversaturated with respect to calcite, dolomite, and most of the silica phases indicating phases undergoing precipitation due to the short time of contact with the minerals or to the gas depletion, or else due to the fluid temperature rise which generates the calcite precipitation (Djidi et al. 2008). Quartz is close to equilibrium in ASS, HN, BH and HDC2. On the other hand, the thermal waters are undersaturated with respect to chalcedony and gypsum indicating phases undergoing dissolution that reflects a long time of contact accelerated by the temperature of the thermal fluid.

Equilibrium state modeling between water and minerals at different temperatures is another approach for estimating thermal reservoir temperatures according to the saturation indices by maintaining the chemical composition constant and varying the temperature (D'Amore et al. 1987; D'Amore and Mejia 1999; Lopez-Chicano et al. 2001) (Fig. 7). In all thermal water samples, calcite was oversaturated at all temperatures which means probably that they are considered as the dominant carbonate minerals (Bozdağ 2016). For sample ASS, calcite and dolomite intersect each other at 160 °C above the equilibrium line indicating a precipitation phase, while the other minerals intersect at temperatures around 100–140 °C below the equilibrium line indicating a dissolution phase due to mixing process between thermal and cold

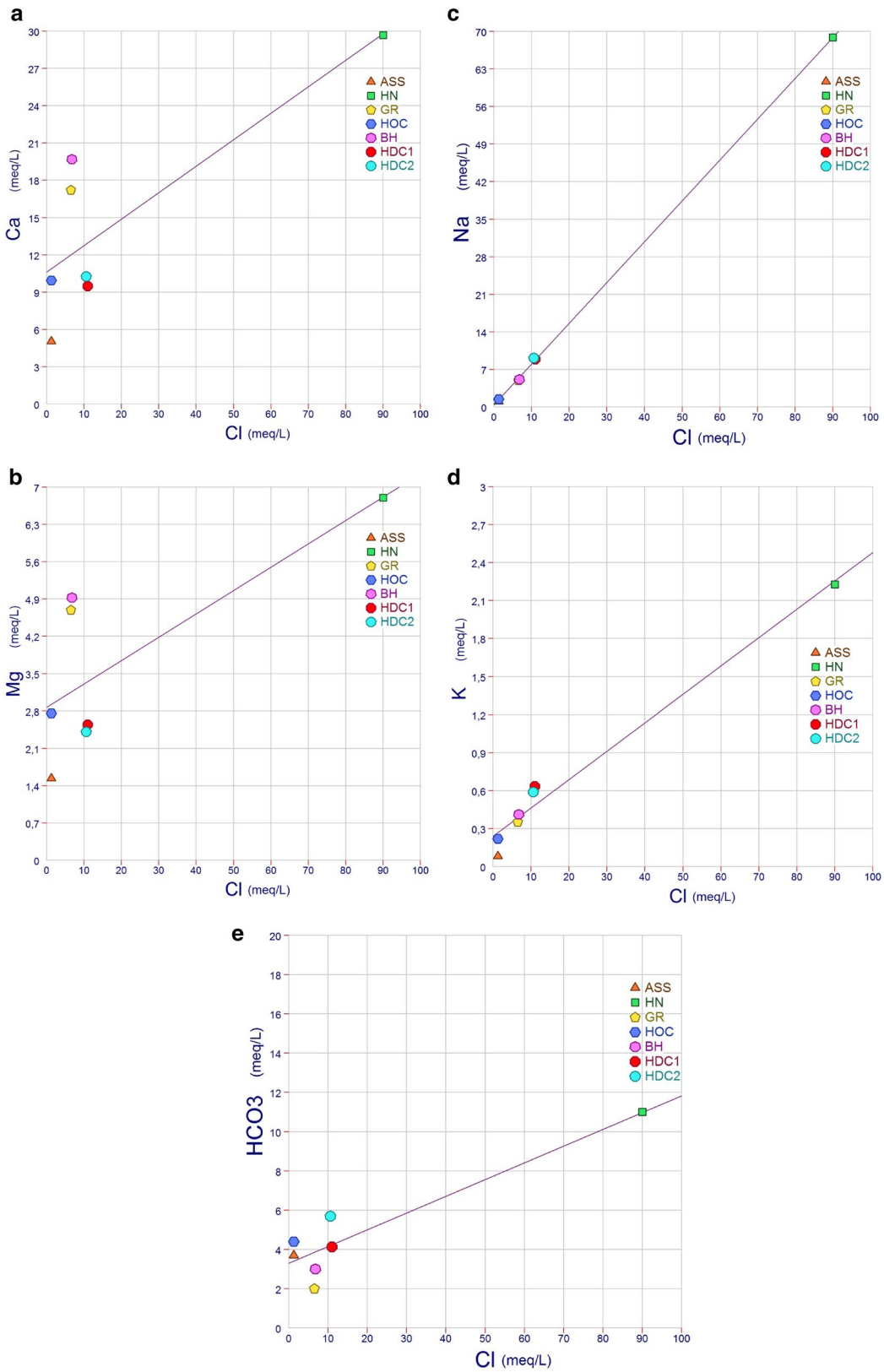

Fig. 4 **a** Ca vs. Cl, **b** Mg vs. Cl, **c** Na vs. Cl, **d** K vs. Cl, **e** HCO_3 vs. Cl scatter diagrams for the northeastern Algerian thermal waters

Table 2 The reservoir temperatures (°C) of thermal waters from the study area using different cationic and silica geothermometers

Samples ID/geothermometers	a (°C)	b (°C)	c (°C)	d (°C)	e (°C)	f (°C)	g (°C)
ASS	23	nd	nd	228	196	161	216
HN	37	nd	nd	141	136	91	170
GR	68	36	19	218	189	153	214
HOC	66	34	17	325	256	237	271
BH	69	37	19	233	199	165	223
HDC1	84	53	34	217	189	153	217
HDC2	81	49	31	207	182	144	210

(a) Quartz (Fournier 1977) $T = [1309/(5.19 - \log SiO_2)] - 273.15$; (b) chalcedony (Fournier 1977) $T = [1032/(4.69 - \log SiO_2)] - 273.15$; (c) cristobalite (α) (Fournier 1977) $T = [1000/(4.78 - \log SiO_2)] - 273.15$; (d) Na–K (Michard 1979) $T = [908/(\log Na/K + 0.7)] - 273.15$; (e) Na–K (Fournier 1977) $T = [1217/(\log Na/K + 1.483)] - 273.15$; (f) Na–K (Truesdell 1976) $T = [855{,}6/(\log Na/K + 0.8575)] - 273.15$; (g) Na–K–Ca (Benjamin et al. 1983) $T = [1416/(1.69 + \log Na/K) + (0.055 * \log \sqrt{Ca/Na})] - 273.15$

nd not determined

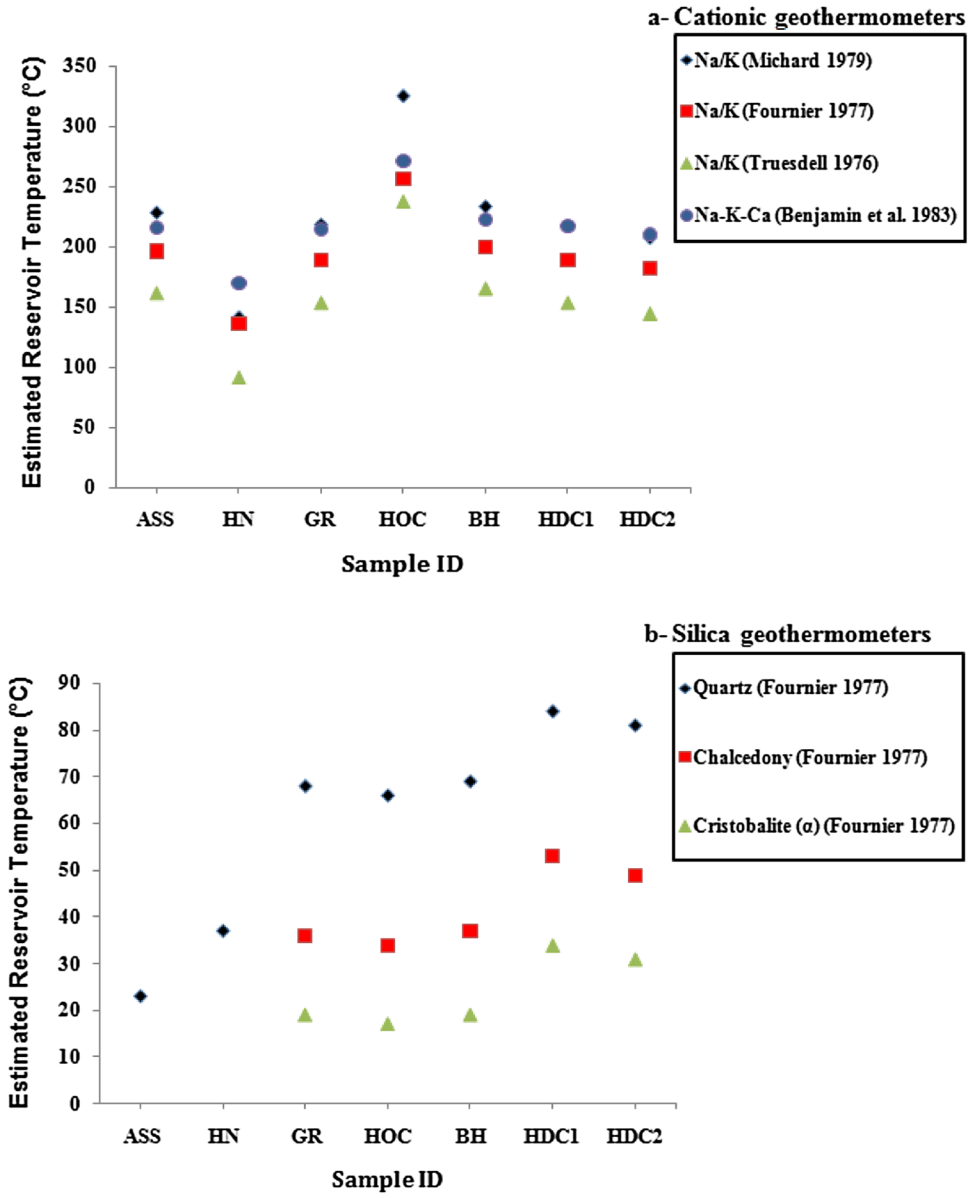

Fig. 5 Estimated reservoir temperatures: **a** Cationic geothermometers, **b** Silica geothermometers

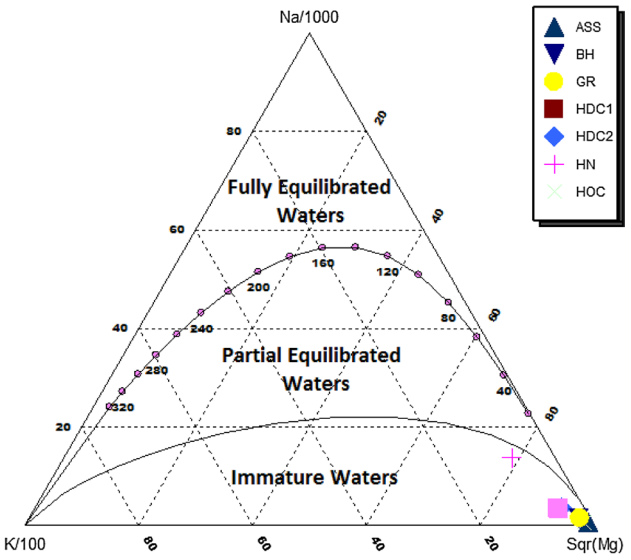

Fig. 6 The Na-K-Mg1/2 triangular diagram of thermal waters from the northeastern Algeria (Giggenbach 1988)

Table 3 Saturation indices with respect to different minerals of the collected thermal waters

Samples ID	Quartz	Chalcedony	Calcite	Dolomite	Gypsum
ASS	− 0.07	− 0.49	0.68	1.01	− 1.47
HN	0.01	− 0.39	1.01	1.64	− 0.74
GR	0.27	− 0.10	0.89	1.45	− 0.43
HOC	0.14	− 0.21	1.25	2.20	− 0.84
BH	0.08	− 0.25	0.94	1.48	− 0.38
HDC1	− 0.10	− 0.36	1.47	2.32	− 0.81
HDC2	− 0.00	− 0.28	1.22	1.91	− 0.83

waters (Fig. 7a). For sample HN, quartz intersects at 40 °C as estimated by quartz geothermometer (Fournier 1977). The other minerals intersect each other at temperatures around 60–100 °C below the equilibrium line and at 160 °C above the equilibrium line (Fig. 7b). At GR sample, dolomite intersects with the equilibrium line at 190 °C while chalcedony, gypsum, and quartz are connected with each other close to the equilibrium line at 80 °C which is close to quartz geothermometer (Fournier 1977) (Fig. 7c). At HOC, chalcedony intersects at 40 °C which is close to the temperature estimated by chalcedony geothermomter (Fournier 1977) (Fig. 7d). For sample BH, chalcedony and quartz cross the equilibrium line SI = 0 at temperatures of 40 °C and 60 °C, respectively. Gypsum crosses the line at 160 °C near to Na/K geothermometer (Truesdell 1976) (Fig. 7e). For samples HDC1 and HDC2, chalcedony intersects the line at 40 °C, quartz crosses it at 80 °C close to quartz geothermometer (Fournier 1977). For the other minerals, calcite and dolomite intersect each other at 150 °C above the equilibrium line (Fig. 7f, g). These results found reveal that thermal waters from the study area are affected by thermal fluids giving a state of non-equilibrium or partial equilibrium at different temperatures from 40 °C to 190 °C which partially overlap with those of quartz and Na/K geothermometers. However, 45–180 °C is considered the most representative reservoir temperature for the study area.

The cold and thermal water samples (Fig. 8) are plotted in stability diagrams for both the Na_2O–Al_2O_3–SiO_2–H_2O (Fig. 8a) and CaO–Al_2O_3–SiO_2–H_2O (Fig. 8b) partial systems. In both diagrams, all thermal samples except ASS are in the stability field of montmorillonite while the cold water samples with ASS are divided between the stability field of kaolinite and montmorillonite. This suggests that kaolinite and montmorillonite are the principal clay minerals interacting with both cold and thermal waters. On the other hand, all of the cold and thermal waters in the study area are contained frequently in an alumino-silicate environment (Gueroui et al. 2014).

Stable isotopes

Stable isotope measurements can be used to determine groundwater circulation based on the isotopic content of atmospheric waters. The isotopic content of thermal waters can also be used to determine the fluid origins in geothermal systems (Craig 1963; White 1986; Matiatos and Alexopoulos 2011). The results of $\delta^{18}O$ and $\delta^{2}H$ are reported in Table 4.

Stable isotope ($\delta^{18}O$ and $\delta^{2}H$) levels for thermal and cold waters throughout the study area are depleted and highly homogeneous. Their values of thermal waters range from − 8.26 to − 6.83‰ for $\delta^{18}O$ and from − 55.23 to − 42.01‰ for $\delta^{2}H$ with respect to V-SMOW. The $\delta^{18}O$ and $\delta^{2}H$ ratio of cold waters ranges from − 7.91 to − 5.50‰ and from − 50.06 to − 33.95‰, respectively, to V-SMOW.

Figure 9a shows the relationship between $\delta^{18}O$ and $\delta^{2}H$ and also the Global Meteoric Water Line of Craig 1961 (GMWL; $\delta^{2}H = 8\ \delta^{18}O + 10$) and the Mediterranean Meteoric Water Line (MMWL; $\delta^{2}H = 8\ \delta^{18}O + 22$) (Gat and Carmi 1970). All the samples taken in the study area are distributed close to the GMWL indicating a meteoric origin of the recharge. On the other hand, most of thermal waters show a lower values of $\delta^{18}O$ and $\delta^{2}H$ than cold waters with the absence of an oxygen shift to positive values in thermal waters suggesting that there has been little isotopic interaction with rocks (Belhai et al. 2016). However, the difference of $\delta^{18}O$ and $\delta^{2}H$ values can be linked to the recharge elevation of thermal waters in comparison to cold waters

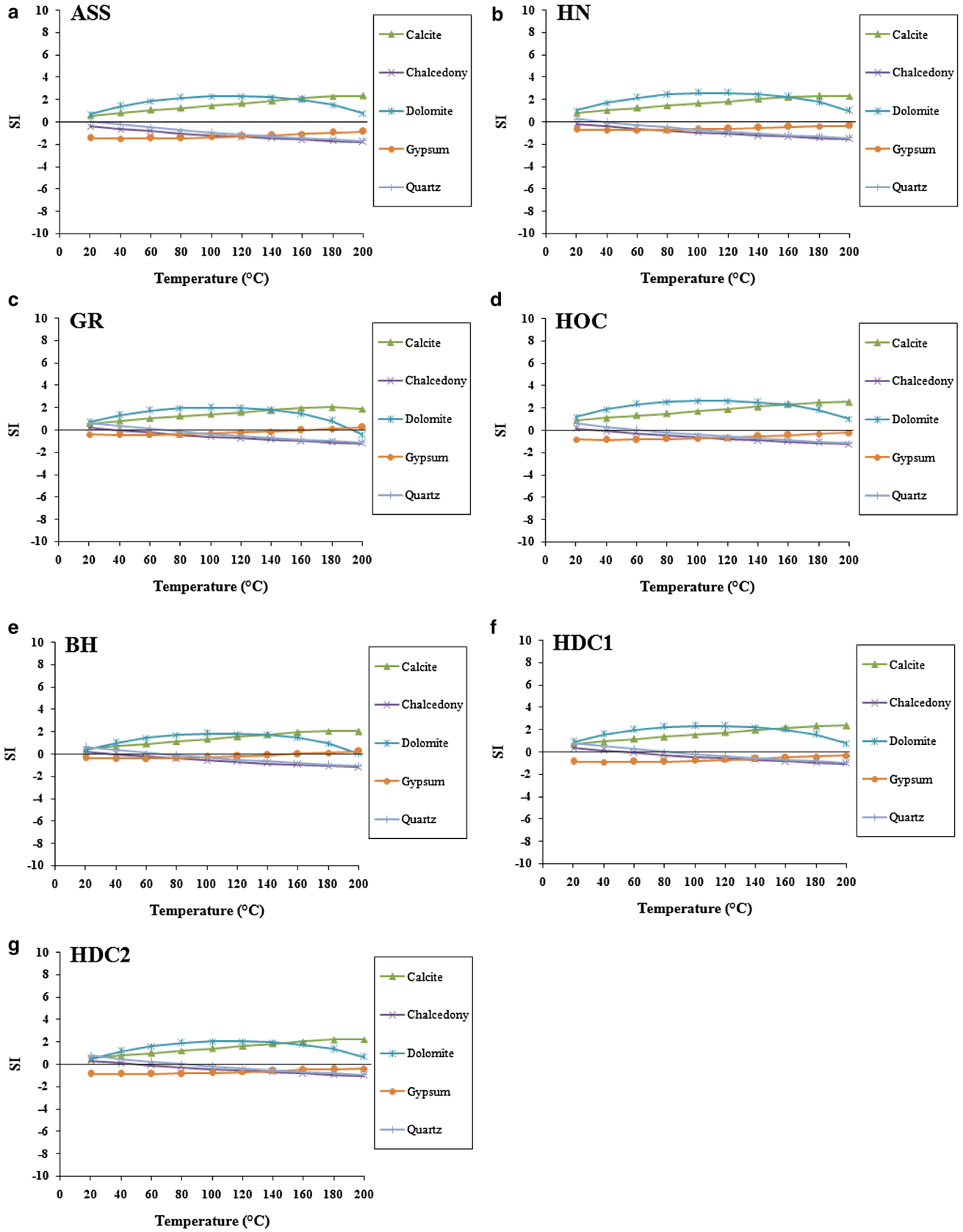

Fig. 7 Mineral equilibrium diagrams for collected thermal waters of the study area: **a** ASS, **b** HN, **c** GR, **d** HOC, **e** BH, **f** HDC1, **g** HDC2

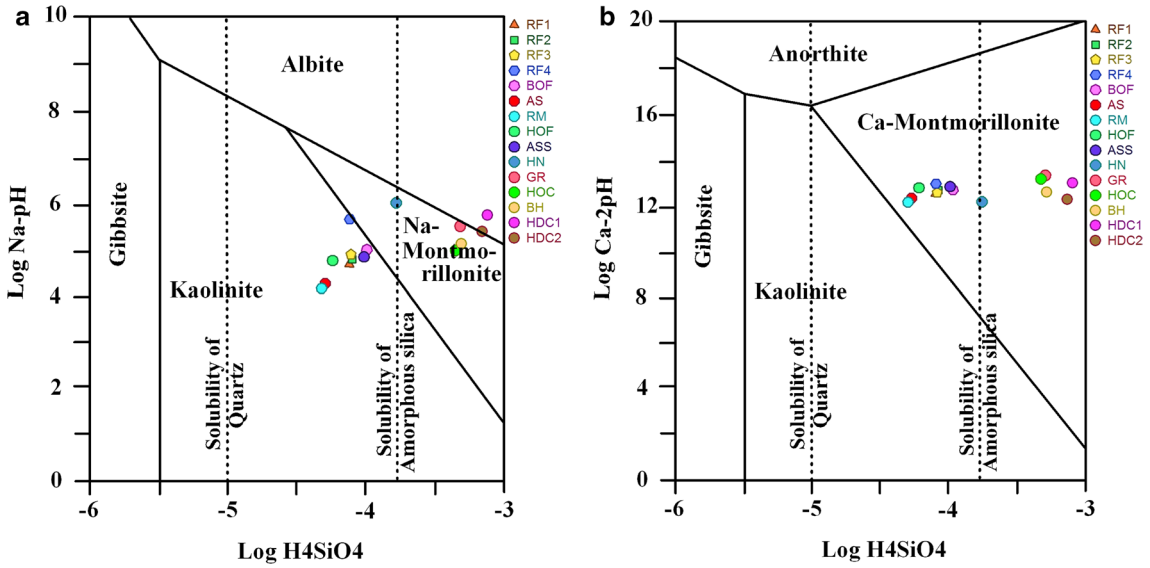

Fig. 8 Plot of cold and thermal water samples in the Na_2O-Al_2O_3-SiO_2-H_2O **(a)** and CaO-Al_2O_3-SiO_2-H_2O **(b)** partial systems at 25°C and 1 atm

(Peñuela-Arévalo and Carrillo-Rivera 2013). Thereby, thermal waters show more negative and a close $\delta^{18}O$ and $\delta^{2}H$ values indicating that these waters have the same recharge area (Bozdağ 2016).

Depletion of $\delta^{18}O$ and $\delta^{2}H$ to negative values in thermal waters (HN, GR, BH, HDC1, HDC2) with generally higher Cl content (~ 200 to 3000 mg/L) indicates at first a mixing process with shallower cold water and that waters have a long time of residence and a deep circulation (Issaadi 1992).

Table 4 Isotopic composition of cold and thermal waters from the study area

Samples ID	$\delta^{2}H$ (‰ V-SMOW)	$\delta^{2}H$ Error	$\delta^{18}O$ (‰ V-SMOW)	$\delta^{18}O$ Error
RF1	− 40.92	±1.0	− 6.55	±0.2
RF2	− 40.30	±1.0	− 6.17	±0.2
RF3	− 38.46	±0.6	− 6.11	±0.2
RF4	− 37.25	±1.3	− 5.76	±0.2
BOF	− 33.95	±0.7	− 5.50	±0.2
AS	− 50.06	±1.0	− 7.91	±0.2
RM	− 48.43	±1.2	− 7.19	±0.2
HOF	− 38.60	±0.6	− 6.46	±0.2
ASS	− 43.29	±0.6	− 7.00	±0.2
HN	− 43.58	±1.3	− 6.83	±0.2
GR	− 54.22	±1.2	− 8.16	±0.2
HOC	− 42.01	±1.4	− 7.02	±0.1
BH	− 55.23	±1.2	− 8.26	±0.2
HDC1	− 46.51	±1.2	− 7.05	±0.2
HDC2	− 49.02	±1.0	− 7.70	±0.2

For cold waters, the slightly higher values of $\delta^{18}O$ and $\delta^{2}H$ than thermal waters and the low Cl content except BOF reveal that these waters have shallow circulation (Fig. 9b, c).

Conceptual model

A conceptual model for different northern geothermal systems (Fig. 10) was constructed according to those proposed by Saibi 2009, Belhai 2017 and Djorfi et al. 2018, who suggest that the geothermal spring emergence is due to deep conductive heat in relation with faults. So, the geothermal system in the study area is recharged through different faults by a deep penetration of infiltrating cold waters (meteoric waters) from Debagh and Debar mountains in the northeast of the study area and Maouna and Maida mountains in the northwest. The infiltrating waters heated at depth flowed upward along faults and fractures through limestone and sandstone formations and mixed with shallow cold waters increasing the different mineral contents of thermal waters.

Conclusion

Thermal water samples collected from northeastern Algeria show high values of TDS (527–6657 mg/L) and EC (709 to 9720 µS/cm) with a neutral pH (7.13–7.84). In the study area, there are three types of thermal waters: the Ca–SO4 is the dominant type in five springs (GR, HOC, BH, HDC1, HDC2), the Na–Cl type in (HN) and the Ca–HCO_3 type in (ASS). These waters appear to be

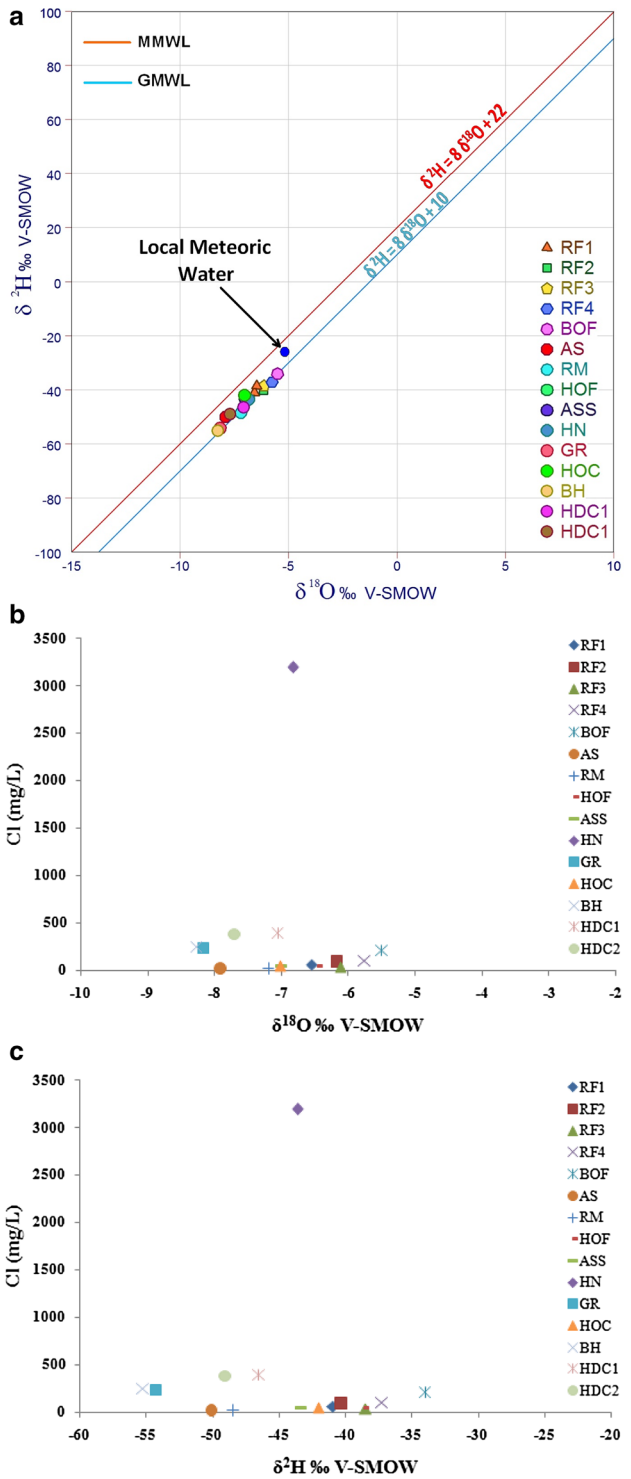

Fig. 9 Isotopic composition of thermal waters: **a** Relationship between $\delta^{18}O$ and $\delta^{2}H$ with the Global Meteoric Water Line (GMWL) and the Mediterranean Meteoric Water Line (MMWL), **b** Relationship between $\delta^{18}O$ and Cl^{-}, **c** Relationship between $\delta^{2}H$ and Cl^{-}

controlled chemically by water–rock interactions and the length of subsurface of the flow paths.

Cationic geothermometers give a large range of high temperatures reaching 325 °C which reflects the dissipation process from the emergence to the surface. The silica geothermometers show a low temperatures between − 17 °C and 84 °C at the origin due to the mixing process. All the thermal waters are immature waters aligned at the magnesium pole in the Giggenbach (1988) diagram reflecting the dilution and mixing process of these waters with cold waters.

The results of mineral saturation show that thermal waters of the study area are oversaturated with respect to calcite, dolomite, and quartz and undersaturated with respect to chalcedony and gypsum indicating phases undergoing precipitation dissolution, respectively. However, these waters are in the state of non-equilibrium or partial equilibrium at different temperatures ranging from 45 to 180 °C.

The stable isotope investigation of thermal and cold waters from the study area reveals a meteoric origin of these waters. Also, the obtained results of $\delta^{18}O$ and $\delta\ ^{2}H$ show a recharge elevation of thermal waters compared to cold waters. Thus, precipitation waters infiltrated through the deep reservoir rocks within faults and became heated by a deep flow moving up to the surface along fractures.

The conceptual model proposes that the geothermal system of the study area is influenced by infiltrating meteoric waters which penetrate deeply through the faults and then heated by a conductive heat flow. The hot waters moved to the surface also through the faults and mixed with cold waters and finally emerge as thermal waters in different sites.

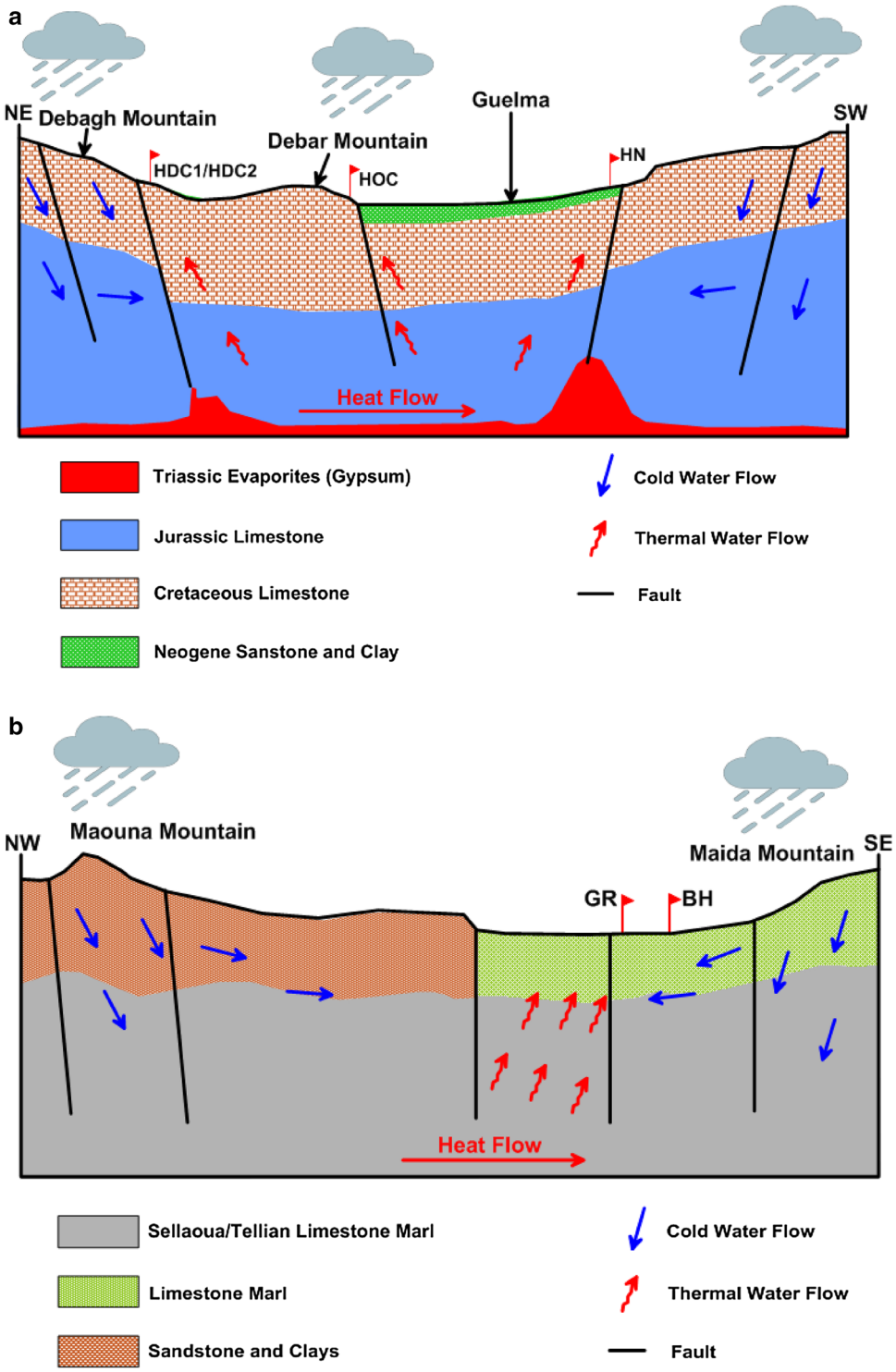

Fig. 10 Conceptual model for the northeastern Algerian thermal waters

References

Alçiçek H, Bülbül A, Alçiçek MC (2016) Hydrogeochemistry of the thermal waters from the Yenice Geothermal Field (Denizli Basin, Southwestern Anatolia, Turkey). J Volcanol Geoth Res 309:118–138

Amarouche-Yala S, Benouadah A, Bentabet AEO, López-García P (2014) Morphological and phylogenetic diversity of thermophilic cyanobacteria in Algerian hot springs. Extremophiles 18(6):1035–1047

ANDI (2013) Agence Nationale de Développement de l'Investissement: Rapport interne, monographie de la wilaya de Guelma, p 19

Asta MP, Gimeno MJ, Auqué LF, Gómez J, Acero P, Lapuente P (2012) Hydrochemistry and geothermometrical modeling of low-temperature Panticosa geothermal system (Spain). J Volcanol Geoth Res 235:84–95

Belhai M, Fujimitsu Y, Bouchareb-Haouchine FZ, Iwanaga T, Noto M, Nishijima J (2016) Hydrogeochemical and isotope geochemical study of northwestern Algerian thermal waters. Arab J Geosci 9(3):169

Belhai M, Fujimitsu Y, Nishijima J, Bersi M (2017) Hydrochemistry and gas geochemistry of the northeastern Algerian geothermal waters. Arab J Geosci 10(1):8

Benjamin T, Charles R, Vidale R (1983) Thermodynamic parameters and experimental data for the Na-K-Ca geothermometer. J Volcanol Geoth Res 15(1–3):167–186

Bouanane-Darenfed A, Fardeau ML, Grégoire P, Joseph M, Kebbouche-Gana S, Benayad T, Ollivier B (2011) *Caldicoprobacteralgeriensis* sp. nov. A new thermophilic anaerobic, xylanolytic bacterium isolated from an Algerian hot spring. Curr Microbiol 62(3):826–832

Bouchareb-Haouchine FZ (1993) Apport de la géothermométrie et des données de forages profonds à l'identification des ressources géothermiques de l'Algérie du Nord. Application à la région du Hodna. Mémoire de Magister, Université d'Alger, Algérie, p 105

Bouchareb-Haouchine FZ, Boudoukha A, Haouchine A (2012) Hydrogéochimie et géothermométrie: apports à l'identification du réservoir thermal des sources de Hammam Righa, Algérie. Hydrol Sci J 57(6):1184–1195

Boudoukha A, Athamena M (2012) Caractérisation des eaux thermales de l'ensemble Sud sétifien. Est algérien. Revue des sciences de l'eau/J Water Sci 25(2):103–118

Bozdağ A (2016) Hydrogeochemical and isotopic characteristics of Kavak (Seydişehir-Konya) geothermal field, Turkey. J Afr Earth Sci 121:72–83

Chouabbi A (1987) Etude géologique de la région de Hammam N'Bails (SE de Guelma, Constantinois, Algérie) (Doctoral dissertation, Thèse de doctorat, Université Paul Sabatier de Toulouse, 1987, 123p)

Craig H (1961) Isotopic variations in meteoric waters. Science 133(3465):1702–1703

Craig H (1963) The isotopic geochemistry of water and carbon in geothermal areas, Nuclear geology on geothermal areas. Spoleto, pp 17–53

D'Amore F, Mejia JT (1999) Chemical and physical reservoir parameters at initial conditions in Berlin geothermal field, El Salvador: a first assessment. Geothermics 28(1):45–73

D'Amore F, Fancelli R, Caboi R (1987) Observations on the application of chemical geothermometers to some hydrothermal systems in Sardinia. Geothermics 16(3):271–282

Deleau P (1952) Le pays constantinois. XIXe Congrès Géologique International

Durand Delga M (1969) Mise au point sur la structure du Nord-Est de la Berbérie. Publ. Serv. Carte géol. Algérie, NS. Bull. soc. Géol. fr.,(7), xiii, 328-337

Dib H (1985) Le thermalisme de l'Est Algérien. Thèse de Doctorat 3ème cycle. PhD thesis, University of Science and Technology Houari Boumedienne, USTHB, Algiers

Djidi K, Bakalowicz M, Benali AM (2008) Mixed, classical and hydrothermal karstification in a carbonate aquifer: Hydrogeological consequences. The case of the Saida aquifer system, Algeria. CR Geosci 340(7):462–473

Djorfi S, Beloulou L, Djorfi S, Djidel M, Guechi S (2018) Hydrothermal characterization of groundwater in the Tamlouka Plain and its surroundings (Northeast Algeria). J Biol Environ Sci 12(2):77–85

Ersoy AF, Sönmez S (2014) Hydrogeochemical and isotopic characteristics of the Ilica geothermal system (Erzurum, Turkey). Environ Earth Sci 72(11):4451–4462

Fournier RO (1977) Chemical geothermometers and mixing models for geothermal systems. Geothermics 5:41–50

Fourré E, Di Napoli R, Aiuppa A, Parello F, Gaubi E, Jean-Baptiste P, Mamou AB (2011) Regional variations in the chemical and helium–carbon isotope composition of geothermal fluids across Tunisia. Chem Geo 288(1–2):67–85

Gat JR, Carmi I (1970) Evolution of the isotopic composition of atmospheric waters in the Mediterranean Sea area. J Geophys Res 75(15):3039–3048

Giggenbach WF (1988) Geothermal solute equilibria. derivation of Na-K-Mg-Ca geoindicators. Geochimica et cosmochimica acta 52(12):2749–2765

Gökgöz A, Akdağoğlu H (2016) Hydrogeology and hydrogeochemistry of a coastal low-temperature geothermal field: a case study from the Datça Peninsula (SW Turkey). Environ Earth Sci 75(15):1143

Gueroui Y, Maoui A, Touati AS (2014) Hydrochemical and bacteriological investigation in groundwater of the Tamlouka Plain, north-east of Algeria. Arab J Geosci 8(5):2417–2432

Issaadi A (1992) Le thermalisme dans son cadre géostructural, apports à la connaissance de la structure profonde de l'Algérie et de ses ressources géothermales. Thèse de doctorat d'état. IST, USTHB

Kecha M, Benallaoua S, Touzel JP, Bonaly R, Duchiron F (2007) Biochemical and phylogenetic characterization of a novel terrestrial hyperthermophilic archaeon pertaining to the genus Pyrococcus from an Algerian hydrothermal hot spring. Extremophiles 11(1):65–73

Kedaid FZ (2007) Database on the geothermal resources of Algeria. Geothermics 36(3):265–275

Kedaid FZ, Mesbah M (1996) Geochemical approach to the Bou Hadjar hydrothermal system (NE Algeria). Geothermics 25(2):249–257

Lahondère JC (1987) Les séries ultra-telliennes d'Algérie orientale et les formations environnantes dans leur cadre structural (Doctoral dissertation, Toulouse 3)

Lahondère JC, Feinberg H, Haq BU (1979) Datation des grès numidiens d'Algérie orientale. C.1. Acad Sci Paris, t1 289:383–386 3fig

Langmuir D (1997) Aqueous environmental geochemistry, vol 549. Prentice Hall, Upper Saddle River

Lopez-Chicano M, Bouamama M, Vallejos A, Pulido-Bosch A (2001) Factors which determine the hydrogeochemical behaviour of karstic springs. A case study from the Betic Cordilleras, Spain. Appl Geochem 16(9–10):1179–1192

Matiatos I, Alexopoulos A (2011) Application of stable isotopes and hydrochemical analysis in groundwater aquifers of Argolis Peninsula (Greece). Isot Environ Health Stud 47(4):512–529

Michard G (1979) Géothermomètres chimiques. Bull BRGM 2:183–189

Michard G (1990) Behaviour of the major elements and some trace elements (Li, Rb, Cs, Sr, Fe, Mn, W, F) in deep hot waters from granitic areas. Chem Geol 89:117–134

Parkhurst DL, Apello CAJ (1999) User guide to PHREEQC (version 2): a computer program for speciation, batch reaction, one-dimensional transport, and inverse geochemical calculations. U.S. Geological Survey, Water Resources Investigations Report 99–4259, p 312

Penna D, Stenni B, Wrede S, Bogaard TA, Gobbi A, Borga M, Fischer BMC, Bonazza M, Charova Z (2010) On the reproducibility and repeatability of laser absorption spectroscopy measurements for δ2H and δ18O isotopic analysis. Hydrol Earth Syst Sci 7:2975–3014

Peñuela-Arévalo LA, Carrillo-Rivera JJ (2013) Discharge areas as a useful tool for understanding recharge areas, study case: Mexico catchment. Environ Earth Sci 68(4):999–1013

Trabelsi S, Makni J, Bouri S, Dhia HB (2015) Hydrochemistry of thermal waters in Northeast Tunisia: water–rock interactions and hydrologic mixing. Arab J Geosci 8(3):1743–1754

Truesdell AH (1976) Summary of section III. Geochemical techniques in exploration. In: Proceeding 2nd UN symposium on the development and use of geothermal resources, San Francisco, 1975, 1, pp liii–lxxix

Verdeil P (1982) Algerian thermalism in its geostructural setting—How hydrogeology has helped in the elucidation of Algeria's deep-seated structure. J Hydrol 56:107–117

Vila JM (1966) Sur la présence d'un flysch allochtone tithonique et néocomien dans la région située entre Bône et Guelma (Est de la chaine numidique, Algérie). CR. somm. Soc. géol. Fr 6:232–233

Vila JM (1970) Le Djebel Edough; un massif cristallin externe du Nord-Est de la Berberie. Bulletin de la Société Géologique de France 7(5):805–812

Vila JM (1980) La chaîne alpine d'Algérie orientale et des confins Algéro-Tunisiens. PhD of Science. University Pierre et Marie Curie, Paris

Vila JM, Ailloud P (1978) Carte structurale au 1: 500,000 de la chaîne alpine d'Algérie orientale et des confins Algéro-Tunisiens

Vila JM, Magne J (1969) Structural setting of Jebel Debbagh-North Constantinnois, Algeria. Bull Soc Géol Fr 7(T. XI):75–81

Vila JM, Busnardo R, Devries A, Magne J, Sigol J (1968) Données stratigraphiques sur la série renversée et charriée du Djebel Bousbaa et étude de son cadre structural (région de Guelma, constantinois, Algérie). B.S.G. Paris France 7(X):206–212

Vila JM, Magne J, Sigol J (1972) Stratigraphie du crétacé autochtone pré-saharien méridional: les séries de Hammam N'Bails et de l'Oued Cheniour. Bull Soc D/Hist Nat de l'AF du N 63:39–49

White AF (1986) Chemical and isotopic characteristics of fluids within the Baca geothermal reservoir, Valles caldera, New Mexico. J Geophys Res Solid Earth 91(B2):1855–1866

Wohletz K, Heiken G (1992) Volcanology and geothermal energy, vol 432. University of California Press, Berkeley